Intravenous transplantation of olfactory bulb ensheathing cells for a spinal cord hemisection injury rat model

Lijian Zhang[1,2,3,*], Xiaoqing Zhuang[4,*] ⓘ, Yao Chen[1,2], and Hechun Xia[1,2]

Abstract

Cellular transplantation strategies utilizing intraspinal or intrathecal olfactory ensheathing cells (OECs) have been reported as beneficial for spinal cord injury (SCI). However, there are many disadvantages of these methods, including additional trauma to the spinal cord parenchyma and technical challenges. Therefore, we investigated the feasibility and potential benefits of intravenous transplantation of OECs in a rat hemisection SCI model. OECs derived from olfactory bulb tissue were labeled with quantum dots (QDs), and their biodistribution after intravenous transplantation was tracked using a fluorescence imaging system. Accumulation of the transplanted OECs was observed in the injured spinal cord within 10 min, peaked at seven days after cell transplantation, and decreased gradually thereafter. This time window corresponded to the blood–spinal cord barrier (BSCB) opening time, which was quantitated with the Evans blue leakage assay. Using immunohistochemistry, we examined neuronal growth (GAP-43), remyelination (MBP), and microglia (Iba-1) reactions at the lesion site. Motor function recovery was also measured using a classic open field test (Basso, Beattie and Bresnahan score). Compared with the group injected only with QDs, the rats that received OEC transplantation exhibited a prominent reduction in inflammatory responses, increased neurogenesis and remyelination, and significant improvement in motor function. We suggest that intravenous injection could also be an effective method for delivering OECs and improving functional outcomes after SCI. Moreover, the time course of BSCB disruption provides a clinically relevant therapeutic window for cell-based intervention.

Keywords

spinal cord injury, olfactory ensheathing cells, OECs, intravenous transplantation, blood–spinal cord barrier, BSCB

Introduction

Traumatic spinal cord injury (SCI) is a devastating event that frequently has disabling outcomes and limited recovery of neurofunction[1,2]. Approximately 15-40 per million people suffer from injuries to the spinal cord every year around the world[3]. However, the current clinically relevant therapeutic strategies for SCI have poor efficacy and undesirable side effects, and efforts are underway to find promising new therapies for this neurological situation[4,5].

Recently, stem cells and other cellular interventions have attracted interest from clinicians and researchers regarding the treatment of SCI. Different sources and types of cells have been and/or are currently being tested in animal experiments or clinical trials. Among these cells, olfactory bulb ensheathing cells (OECs) have emerged as an encouraging cell candidate for transplantation therapies to promote axonal regeneration after SCI due to their capability to promote axonal regeneration[6,7], provide trophic support to injured host cells[8,9], and modulate inflammatory reactions[10]. Based

[1] Department of Neurosurgery, General Hospital of Ningxia Medical University, Yinchuan, Ningxia, China
[2] Ningxia Human Stem Cell Research Institute, General Hospital of Ningxia Medical University, Yinchuan, Ningxia, China
[3] Surgery Laboratory, General Hospital of Ningxia Medical University, Yinchuan, China
[4] Department of Nuclear Medicine, General Hospital of Ningxia Medical University, Yinchuan, Ningxia, China

* Both the authors are co-authors and contributed equally to this article

Corresponding Authors:
Hechun Xia, Department of Neurosurgery, Department of Neurosurgery, General Hospital of Ningxia Medical University, No. 804 Shengli Steet, 750004, Yinchuan, China.
Email: xhechun@nyfy.com.cn

on their intrinsic myelinating potential, OECs can also form myelin sheaths, which encapsulate neurons to support the growth of neurites[11].

OECs can be isolated from the nerve fiber layer of the olfactory bulb as well as the lamina propria of the olfactory mucosa. Olfactory mucosa OECs are easily accessed for autologous transplantation with a minimally invasive procedure[12], while olfactory bulb OECs may have higher potential to promote neuroregeneration[13]. This greater function benefit over mucosal cultures might be due to their ability to mediate regeneration of severed axons across the injury site[14,15]. Direct evidence has also shown that olfactory bulb OECs could be seen as myelin-forming cells, which have more robust ability compared with olfactory mucosa OECs based on their different microscopic morphological properties[16]. The functional benefits of olfactory bulb OECs have been proposed for the treatment of SCI in a range of adult mammals, including rodents[17], nonhuman primates,[18] and human patients[19]. Minimally invasive procedures for harvesting the olfactory bulb OECs in human subjects have been developed[20,21]. Moreover, Liadi et al. have demonstrated that storing olfactory bulb tissue before culture could be achieved without compromising the viability of cells, which makes it possible to obtain a large number of cells for the clinic use of autologous, particularly allogeneic, OEC transplants[22]. Cell-based therapy via the intravenous route is convenient and noninvasive to apply in clinical practice compared with intraspinal or intrathecal transplantation. A body of findings has shown that olfactory bulb OECs could express a number of growth factors to stimulate regeneration in the injured central nervous system (CNS) in a paracrine and autocrine manner[23]. Therefore, we assume that intravenous administration of olfactory bulb OECs could facilitate the neuroregenerative process in the injured spinal cord.

The in vivo cellular behaviors of the grafted OECs lead to more complex conditions than the well-controlled situation of in vitro experiments. Detailed information about the fate of transplanted cells in vivo is limited but could help reveal their neuroprotective roles and promote the translation of cell transplantation into clinical settings in the treatment of SCI[24]. Various cellular imaging modalities are used, based on different types of labeling agents (i.e., superparamagnetic iron oxide nanoparticles or ^{99m}Tc), some of which have already been applied in clinical conditions[25,26]. However, compared with magnetic resonance imaging (MRI) or nuclear imaging, optical imaging is more favored for biological applications that require high-resolution cellular imaging and long-term observation to track transplanted cells[27,28]. Quantum dots (QDs), with unique optical properties, such as size-dependent tunable emission, high photostability, and high quantum yield, are appealing as molecular probes for cell tracking[29].

In this study, QD-labeled olfactory bulb OECs were intravenously transplanted into a spinal cord hemisection injury rat model. Fluorescence imaging was employed to track the migration of OECs in the injured spinal cord. The therapeutic effects of OECs in SCI were also investigated.

Materials and Methods

OEC Cultures and Labeling

OECs were isolated from the olfactory bulbs of adult male Sprague-Dawley (SD) rats (eight weeks, Ningxia Medical University, Laboratory Animal Center) as previously described[30]. Briefly, after removal of the pia, the nerve fiber and glomerular layers of the olfactory bulbs were dissected and minced into small pieces in chilled Hank's balanced salt solution (HBSS) (Invitrogen, Carlsbad, CA, USA) and then trypsinized (0.1% w/v Type IX trypsin (Sigma, St. Louis, MO, USA), 15 min each, 37 °C, 5% CO_2). The dissociated cells were washed and resuspended in complete medium consisting of Dulbecco's modified Eagle medium (DMEM)/Ham's/F-12 (1:1 mixture, Gibco, Invitrogen, Carlsbad, CA, USA) supplemented with 10% fetal bovine serum (FBS). After incubation on uncoated petri dishes for 54 hours, OECs collected from the final supernatant were seeded onto poly-L-lysine (Sigma)-coated slides and maintained in an incubator (37 °C, 5% CO_2) for eight days after purification, and the medium was changed every two days. The morphology and immunostaining characteristics of the purified OECs were determined in our previous study[31].

On the day before cell transplantation, OECs were labeled with QDs (Mesolight, Suzhou, China) by direct endocytosis[32]. Briefly, OECs were grown to 85% confluence on polystyrene tissue culture dishes. After medium removal, the cells were washed twice in PBS. Then, serum-free cell culture medium containing 20 nM QDs was added to cells for two hours at 37 °C. After removal of the medium containing QDs, the cells were washed twice in PBS and then further incubated in complete cell culture medium for up to 24 hours.

To enable the observation of the intracellular distribution of QDs in cultured OECs, the OECs were labeled with 1 μmol/L calcein acetoxymethyl ester (calcein AM; Invitrogen, Waltham, MA, USA) and the nuclei were stained with DAPI (Beyotime, Shanghai, China). To examine subcellular localization of the QDs, cells were treated with organelle trackers including Lyso Tracker® Green DND-26, Mito Tracker® Green FM, and ER-Tracker™ Blue-White DPX (Invitrogen, Waltham, MA, USA) following the manufacturer's instructions. Confocal fluorescence images were acquired with an Olympus confocal imaging system (Olympus FV100, Olympus, Japan).

Cytotoxicity Analysis

Cytotoxicity measurements were performed with well-characterized OECs in 96-well plates. Cells suspended at a density of 4×10^4 cells/mL were prepared by appropriate dilution with medium. A total of 100 μL of cell suspension was transferred to each well, and the cells were incubated overnight in DMEM and 10% FBS. After cell adhesion, the medium was removed and replaced with 10 μL of fresh medium doped with modified QDs at concentrations of 10
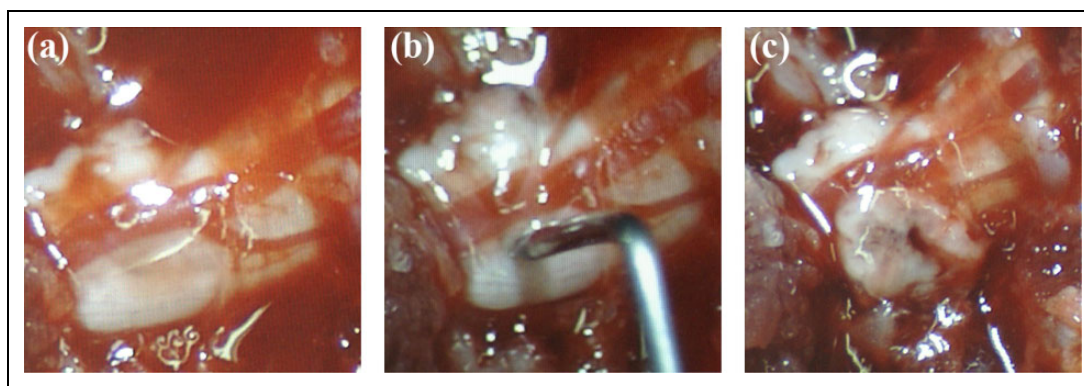
Figure 1. Establishment of rat spinal cord hemisection model. (a) Before injury; (b) spinal cord hemisection; (c) after injury.

nM, 20 nM, and 50 nM; the control group was not exposed to QDs. After 24 hours of incubation with the QDs, the cell culture medium with the QDs was removed and replaced with 100 μL of fresh medium (without phenol red). Then, 10 μL of MTT solution (Beyotime, Shanghai, China) was added to each well, and the cells were incubated for three hours without exposure to light. The optical density (OD) was measured at 570 nm with a BIO-RAD M-450 microplate reader (Bio-Rad iMARK, Hercules, CA, USA).

Experimental Animals

All protocols were approved by the Ningxia Medical University Animal Ethics Committee (2018-054). Adult male SD rats (weight, 320–350 g) were used in this study. The animals were housed in individual ventilated cages (one rat per cage) under consistent temperature (21 ± 1.2 °C) and humidity (55 ± 5.0%) conditions with a 12-hour light/dark cycle. The rats were fed standard rodent chow and drinking water ad libitum.

Establishment of the SCI Rat Model

Rats were anesthetized with ketamine and xylazine (80 mg/kg and 10 mg/kg, respectively), and body temperature was maintained using a heating pad. The skin over the upper thoracic area was shaved and cleaned with a betadine solution. The skin was incised, and then the connective and muscle tissue were bluntly dissected to expose the twelfth thoracic (T12) vertebral body. Then, a lateral hemisection was performed at T12. A needle (26G) was used to establish a lateral hemisection. The needle was bent by 90° with the end in 5 mm. Initially, an angled needle punctured the spinal cord dorsoventrally at the midline while avoiding the arteriae spinalis anterior, and it was then pulled to cut the left half of the spinal cord (Figure 1). This operation was repeated three times to ensure completeness of the hemisection[33]. Finally, the lesion was closed in layers with individual sutures. Appropriate post-operative care was provided for all operated rats. Bladders of the SCI rats were manually expressed three times daily until the bladder function was restored. For pain management, buprenorphine (0.05 mg/kg) was administered subcutaneously every 12 h for three consecutive days after trauma[34].

Experimental Groups

In total, 147 adult male SD rats were randomly assigned to the following experimental groups: (1) cord hemisection with intravenous transplantation of QD-labeled OECs at 24 hours after the establishment of the SCI model (SCI/OEC, n = 5 rats per time point); (2) cord hemisection and grafted with QD solution at 24 hours after the establishment of the SCI model (SCI/QD, n = 5 rats per time point); (3) normal spinal cord and grafted with QD-labeled OECs (control group, n = 5 rats per time point); (4) normal spinal cord and injected with Evans Blue (EvB) solution (n = 3 rats per time point); (5) cord hemisection and grafted with EvB solution one day after the establishment of the SCI model (n = 3 rats per time point) (Figure 2).

Cell Transplantation

OECs were prepared in 1 mL cell culture medium per 1×10^6 cells. One day after the establishment of the SCI model, OECs were injected intravenously via the tail vein within one minute, and 1 ml of 20 nM QD solution diluted with cell culture medium was also intravenously injected into the hemisection SCI model as a comparison group. For control animals, 1 ml of OECs was intravenously injected into normal rats.

Behavioral Testing

All the cord-hemisected rats in groups 1 (SCI/OEC) and 2 (SCI/QDs) were observed for any recovery of motor activity. Behavioral evaluation was performed daily in an open field
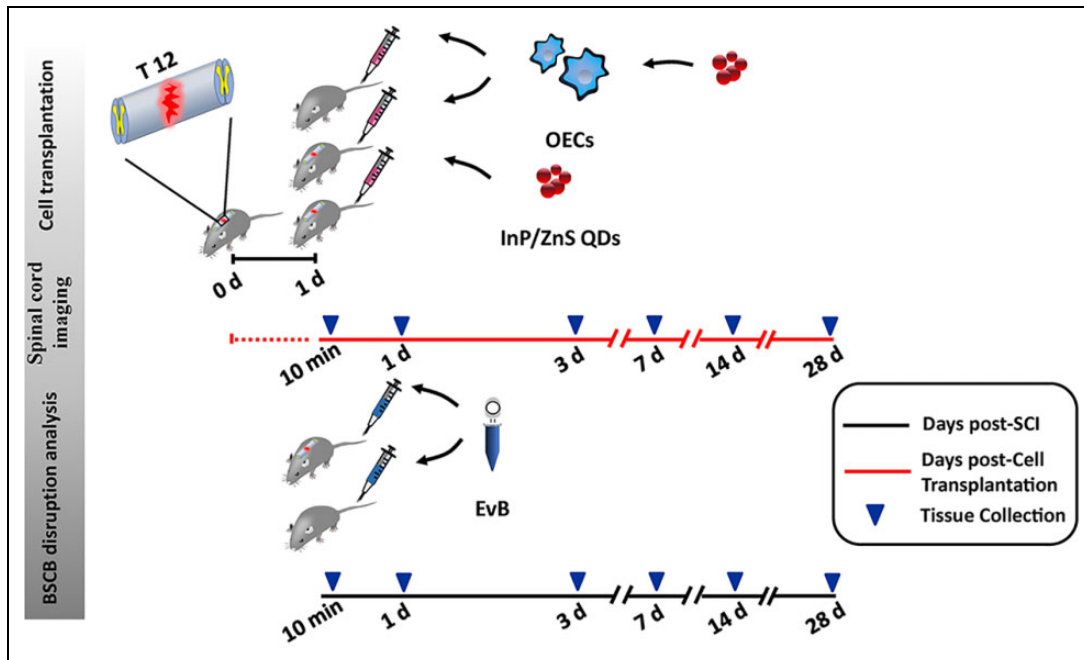
Figure 2. Experimental scheme for tracking the QD-labeled OECs in SCI rats.

according to the Basso, Beattie and Bresnahan (BBB) rating scale up to 28 days post-cell transplantation[35,36].

Ex Vivo Optical Imaging

Rats were sacrificed with euthanasia and perfused with saline at 10 min, one hour, one day, three days, seven days, 14 days, and 28 days after cell injection. Spinal cords and organs (livers, lungs, heart, spleen, kidney, and intestines) were quickly extracted and imaged with an optical/X-ray imaging system (Bruker, Karlsruhe, Germany). Fluorescence images were captured at 5 s with the excitation and emission wavelengths set at 530 nm and 600 nm, respectively, and the following settings: f-stop = 8.08; X-binning = ×2; Y-binning = none. The parameters ($p/s/mm^2/sr$) were obtained by measuring the median fluorescence intensity (MFI) via the manufacturer's data processing software.

Characterization of BSCB Permeability with EvB

Uninjured or hemisected rats were injected with 1 mL of 4% solution of EvB (2.50 mg/kg) into the tail vein at 10 min, one hour, one day, three days, seven days, 14 days, and 28 days post-SCI. EvB was allowed to circulate for 30 min, after which the rats were transcranially perfused with saline. Spinal cords were removed with the meninges stripped, and the EvB distribution was assessed by ex vivo imaging using the optical/X-ray imaging system (Bruker, Karlsruhe, Germany) with the excitation and emission filters set at 610 nm and 670 nm, respectively. For a direct comparison of the EvB fluorescence intensity between spinal cords, all images were taken with a 0.25 s exposure and normalized to the

intact condition by adjusting the aggregate color scale to min = 2.00×10^5 and max = 3.50×10^9.

To quantify the EvB dye contents, 1 cm segments of the spinal cord centered on the injury site were removed, weighed, homogenized in 7.5% (w/v) trichloroacetic acid, and centrifuged for 10 min at 10,000 rpm, 4 °C. Colorimetric measurements of the supernatant were performed using a microplate reader (620 nm, Bio-Rad iMARK, USA). The EvB concentration was calculated based on a standard curve of EvB in trichloroacetic acid (data reported as EvB per spinal cord weight: μg/g).

Immunohistochemical Assay and Hematoxylin and Eosin (HE) Staining

All rats were deeply anesthetized with sodium pentobarbital (25 mg/kg) and perfused with saline. Spinal cord sections from the tenth thoracic segment were dissected totally and fixed in 10% formalin and embedded in paraffin using routine procedures[37]. Serial transverse sections (5 μm) were cut from paraffin blocks and stained with HE for histopathologic examination under a light microscope (Leica DM4000 M, Wetzlar, Germany).

To investigate the neuroprotective roles of OEC on the injured spine, immunohistochemistry assays were performed. Sections were incubated with the following primary antibodies: anti-Myelin Basic Protein (MBP) antibody (1:50, Abcam, ab7349, Cambridge, MA, USA), anti-Iba-1 antibody (1:50, Abcam, ab139590, Cambridge, MA, USA), anti-GAP-43 antibody (1:500, Abcam, ab16053, Cambridge, MA, USA) and anti-p75 nerve growth factor receptor
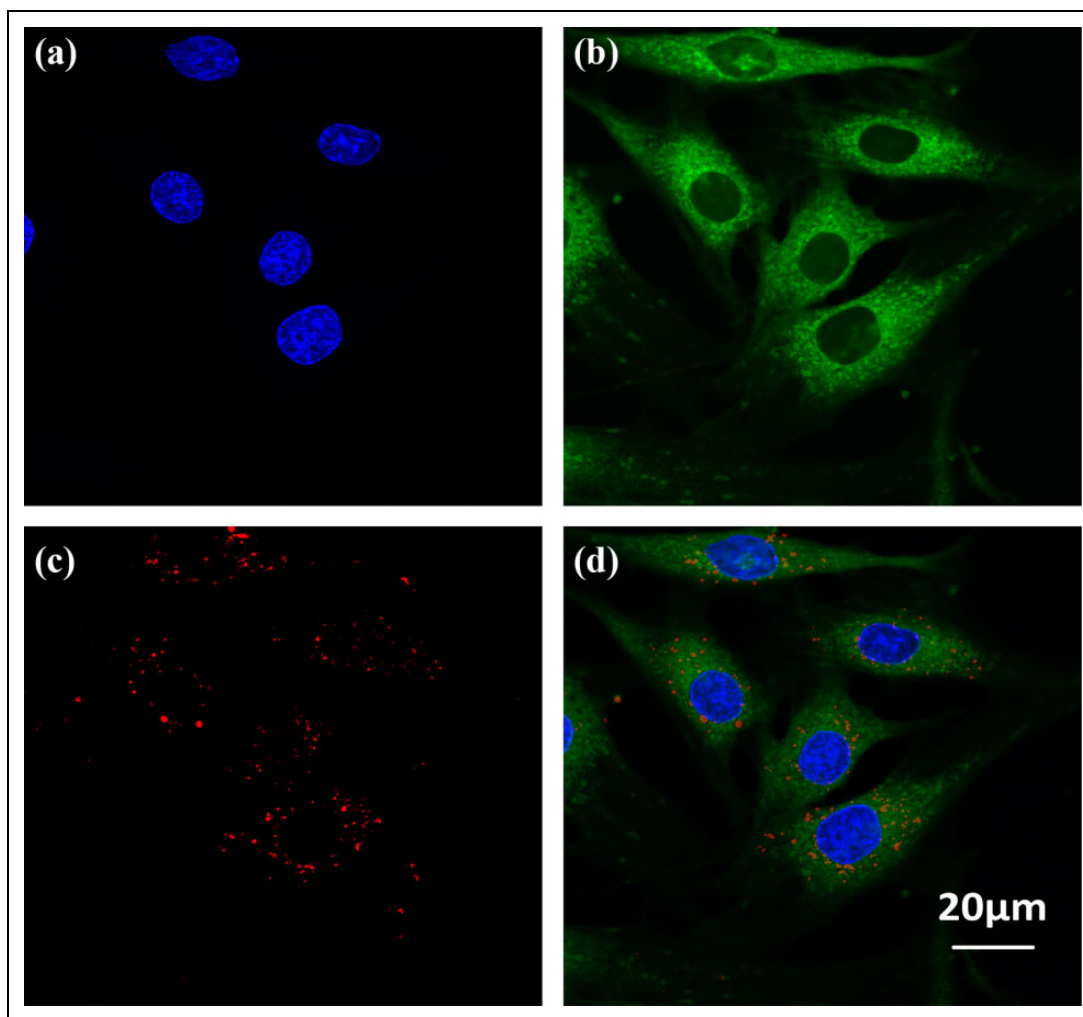
Figure 3. Confocal microscopic images of OECs labeled with QDs. (a) Cell nuclei stained with DAPI (blue stain). (b) The morphology of OECs shown by calcein AM staining (green stain). (c) Fluorescence images of OECs labeled with QDs (red stain). (d) The overlaid images of (a), (b), and (c) (scale bar = 20 μm).

(NGFR) antibody (1:500, Abcam, ab7349, Cambridge, MA, USA). The sections were then incubated with biotinylated goat anti-rabbit IgG followed by streptavidin-peroxidase. Finally, we obtained the immunohistochemistry images under a light microscope (Leica DM4000 M, Germany) at a magnification of 200. Average values of integrated optical density (IOD) were obtained from three random fields per slide using Image-Pro Plus software (Media Cybernetics, Rockville, MD, USA).

Statistical Analysis

All values shown here are expressed as the mean $\pm$ standard deviation, and all statistical analyses were performed with GraphPad Prism Software (GraphPad Software, La Jolla, CA, USA) using one-way analysis of variance (ANOVA) with Tukey's post hoc test for multiple comparisons. Correlation analysis was performed using Pearson's product

moment (r) correlation. $p < 0.05$ was considered statistically significant.

Results

QD Labeling of OECs

Confocal microscopy was used to determine whether OECs were labeled with QDs. Strong red fluorescence from QDs was observed. The QDs localized mainly at a juxtanuclear location inside OECs (Figure 3). Following these observations, we also investigated the subcellular localization of QDs in OECs. After QD labeling, OECs were incubated with dyes that probe intracellular organelles, including the endoplasmic reticulum (ER), mitochondria (Mito), and lysosomes (Lyso). Fluorescence microscope images showed that the QDs were nonspecifically distributed in endosomes and mostly entrapped by the ER (Supplementary Figure 1).
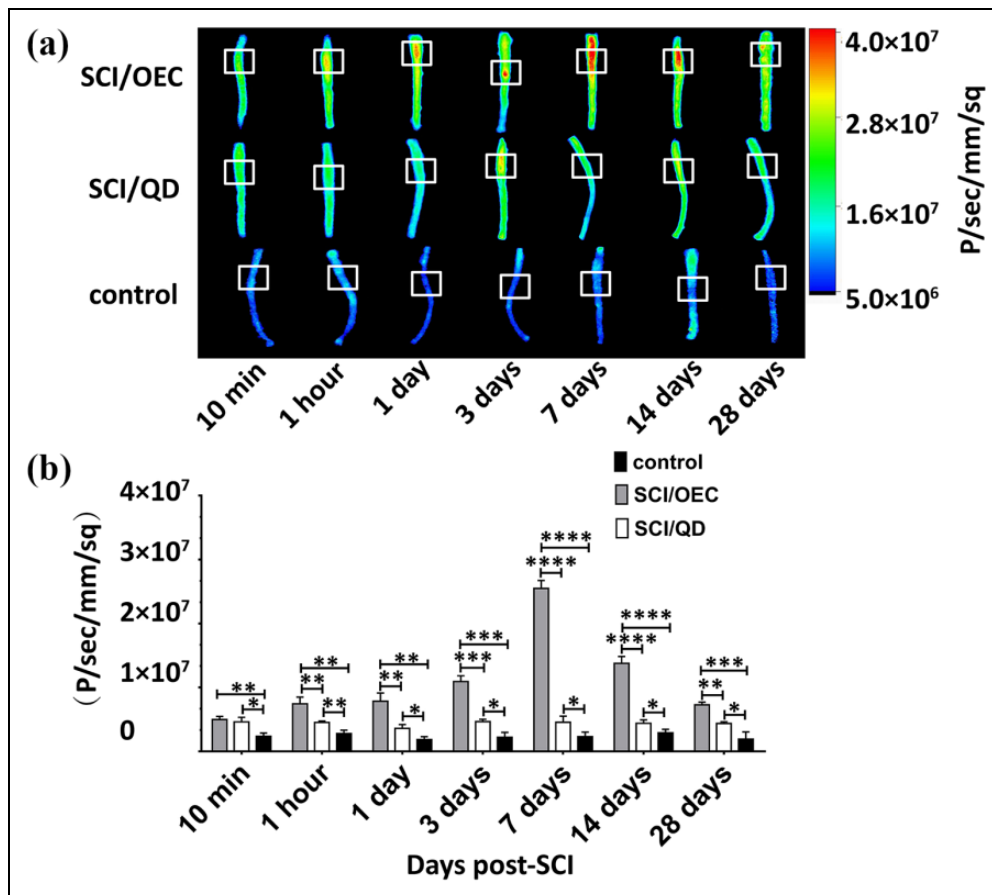
Figure 4. The distribution of QD-labeled OECs in the injured spinal cords. (a) Fluorescence images of isolated spinal cord from the control group, SCI/QD group, and SCI/OEC group. (b) Measurement of the fluorescence signal in the lesion site (shown with white box) at different time points post-OEC transplantation.*$p < 0.05$; **$p < 0.01$; ***$p < 0.001$; ****$p < 0.0001$.

Cytotoxicity Tests of QDs

The cytotoxicity of QDs was evaluated by a trypan blue exclusion assay. Over 93% of OECs were viable and did not significantly differ from their unlabeled counterparts when treated with less than 20 nM QDs, indicating that QD labeling did not significantly affect cell viability. However, significant cytotoxicity was observed when the OECs were transduced with 50 nM QDs ($p = 0.016$; n = 3) (Supplementary Figure 2). Therefore, in the following experiment, we used 20 nM QDs to label OECs.

Accumulation of QD-Labeled OECs in the Injured Spinal Cord

The data showed that the QD-labeled OECs were located in the injured spinal cord as early as 10 min (4.97×10^6 p/s/mm^2/sr) after cell injection. The peak signal (2.55×10^7 p/s/mm^2/sr) occurred seven days after cell infusion, which corresponded to the accumulation of QD-labeled cells around the injury sites. At 28 days after cell injection, the QD-labeled OECs were still observed in the spinal cord but

with a dramatically reduced signal (7.28×10^6 p/s/mm^2/sr) (Figure 4). Compared with the control group, the SCI/OEC group had statistically significantly higher fluorescence intensities at every studied time point ($p < 0.0001$; n = 5). With the exception of 10 min post-transplantation, the fluorescence intensities of the SCI/OEC group were significantly higher than those of the SCI/QD group ($p = 0.0088$, 0.0066, 0.0004, 0.0001, 0.0002, and 0.0006, respectively; n = 5).

The rats were sacrificed to examine the biodistribution of fluorescence in the organs. As shown in Supplementary Figure 3, the fluorescence mostly accumulated in the livers, stomach, and intestine, followed by kidney, lungs, and heart, and the lowest accumulation was found in the spleen. In the SCI/OEC group, the fluorescence intensity in the livers was higher than that in the SCI/QD and control groups.

Quantification of EvB Leakage after SCI using ex Vivo Imaging

Here, we investigated the spatial and temporal changes in BSCB permeability from 10 min to 28 days after hemisection SCI. Ex vivo imaging showed that SCI-induced EvB
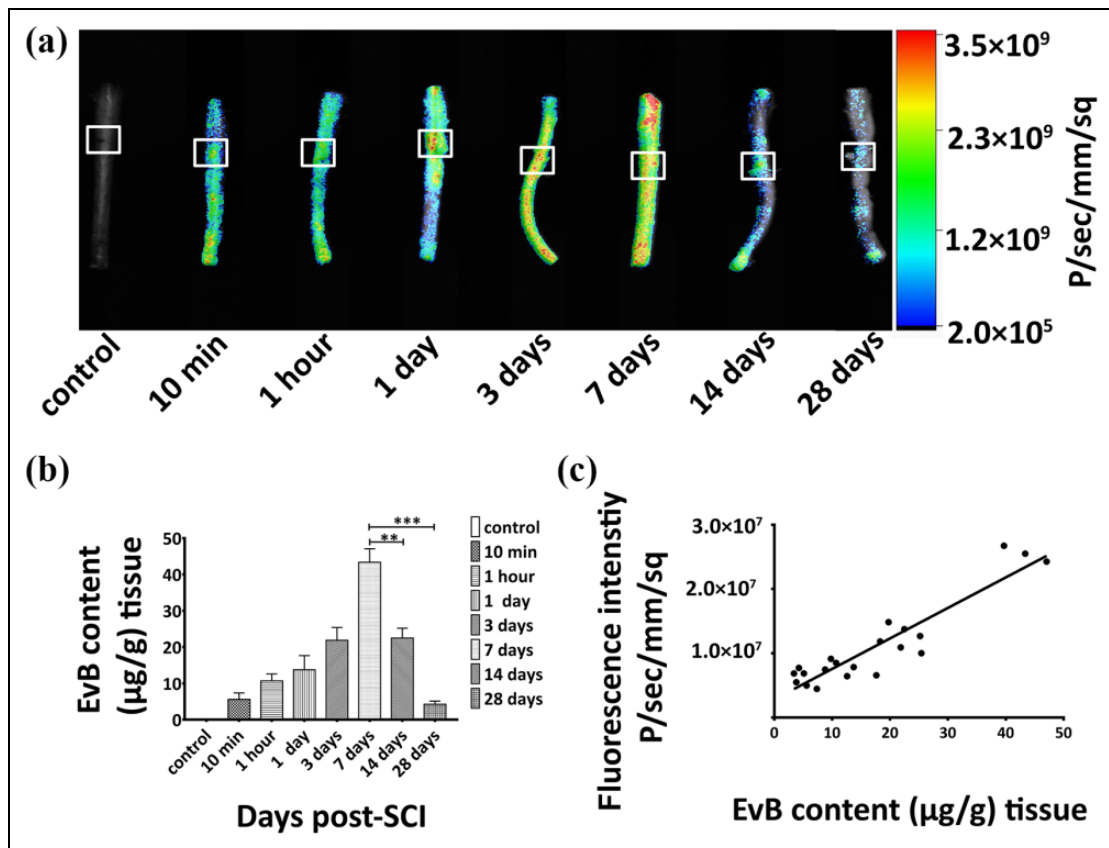
Figure 5. BSCB permeability analysis after SCI. (a) Ex vivo optical image of EvB dye extravasation of the normal control, 10 min, one hour, one day, three days, seven days, 14 days, and 28 days post-SCI at T12. The lesioned site is shown with a white box. (b) Quantification of EvB concentration in the lesion blocks at 10 min, one hour, one day, three days, seven days, 14 days, and 28 days post-SCI (*$p < 0.05$; **$p < 0.01$; ***$p < 0.001$). (c) Pearson's correlation analysis between EvB leakage and fluorescence intensity in the injured spinal cord ($p < 0.0001$; $R^2 = 0.8589$).

dye leakage could readily be observed within minutes (10 min) and persisted for at least 28 days post-SCI at the injured site (Figure 5(a)). At one day after SCI, EvB fluorescence centered at the injured site. At three days and seven days after SCI, the areas of EvB leakage were expanded rostrally and caudally to the lesion epicenter with increased fluorescence intensities. At 14 days and 28 days after SCI, the EvB fluorescence intensities at the lesion site were markedly reduced but still detectable.

To quantify the extent of BSCB leakage, EvB was extracted from a 1 cm segment of the spinal cord tissue at the injury site and measured by spectrophotometry. The results showed a biphasic pattern of BSCB disruption in this study period (Figure 5(b)). The EvB dye concentration in the lesion block increased markedly at three days and seven days and peaked at seven days after SCI (8.04 ± 1.22 and 10.67 ± 1.91 µg/g tissue; n = 3, respectively). At 14 days and 28 days after SCI, the EvB contents significantly decreased compared with those at seven days after SCI (4.25 ± 0.85, n = 3; and 1.30 ± 0.66 µg/g tissue, n = 3, $p = 0.0059$ and 0.0013, respectively). Figure 5(c) shows that there was a positive correlation between fluorescent signal detected in

the OEC-treated spinal cord and the EvB leakage in the damaged spinal cord ($p < 0.0001$, $R^2 = 0.8589$).

Pathology Analysis of Injured Spinal Cords

HE staining results of the spinal cord from different groups are shown in Figure 6, and the effect of OECs on preservation of anterior horn motor neurons in the spinal cord was also investigated. Compared with the control group, the anatomical structure of the spinal cord at one day post-transplantation (two days post-SCI) was severely disordered, with a significantly reduced number of anterior horn motor neurons in both the SCI/OEC (52.75 ± 4.53 vs. 16.41 ± 3.24, $p < 0.0001$; n = 5) and SCI/QD group (52.75 ± 4.53 vs. 11.92 ± 2.53, $p < 0.0001$; n = 5). From three days to 28 days after transplantation, the OEC treatment induced a significant increase in anterior horn motor neurons. The significant difference between SCI/OEC and SCI/QD groups began at three days after OEC transplantation (22.58 ± 2.57 vs. 14.65 ± 3.80, $p = 0.003$; n = 5). In the SCI/OEC group, a near-regular tissue structure with no obvious necrosis or vacuoles in the gray and white matter was apparent at
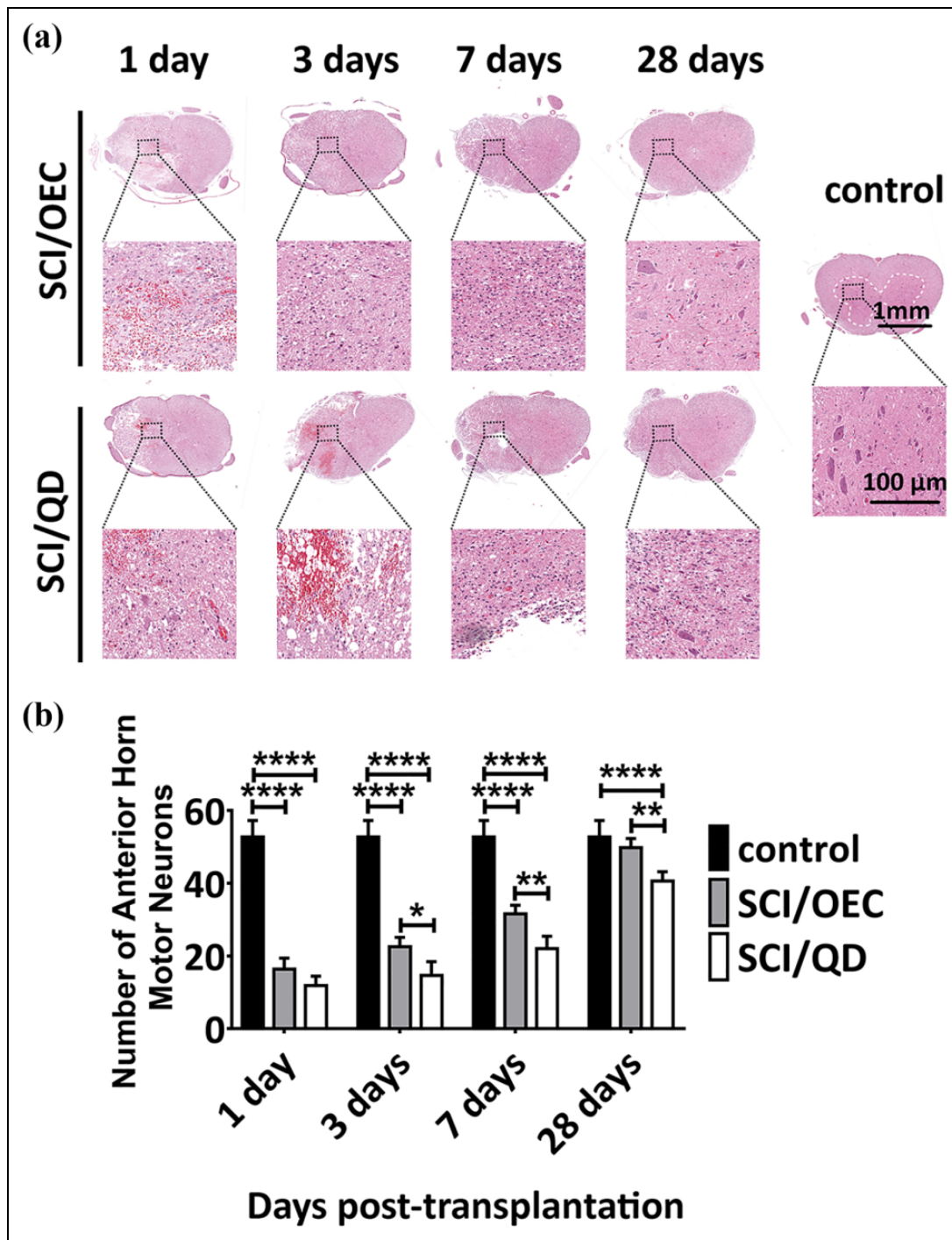
Figure 6. The survival and preservation of anterior horn neurons after OEC treatment. (a) HE staining in the SCI/OEC, SCI/QD, and control group at one day, three days, seven days, and 28 days after transplantation. (b) Quantitative analysis of the number of anterior motor neurons. Data are presented as mean $\pm$ SD, n = 5 per group. *p < 0.05; **p < 0.01; ***p < 0.001; ****p < 0.0001; scale bar = 100 μm, applicable to all sections.

seven days post-transplantation. Anterior horn motor neurons were remarkably preserved when compared with the SCI/QD group (31.59 ± 2.39 vs. 22.02 ± 3.42, $p = 0.003$; n = 5). However, the number of motor neurons in the SCI/OEC group was still significantly lower than that in the control group (52.75 ± 4.53 vs. 31.59 ± 2.39, $p < 0.001$; n = 5). No significant difference was observed in rats between the control group and the SCI/OEC group at 28 days post-transplantation (52.75 ± 4.53 vs. 49.79 ± 2.53, $p = 0.064$; n = 5). An extensive loss of motor neurons was still found in the SCI/QD group compared with the control group (52.75 ± 4.53 vs. 40.60 ± 2.57, $p < 0.001$; n = 5).
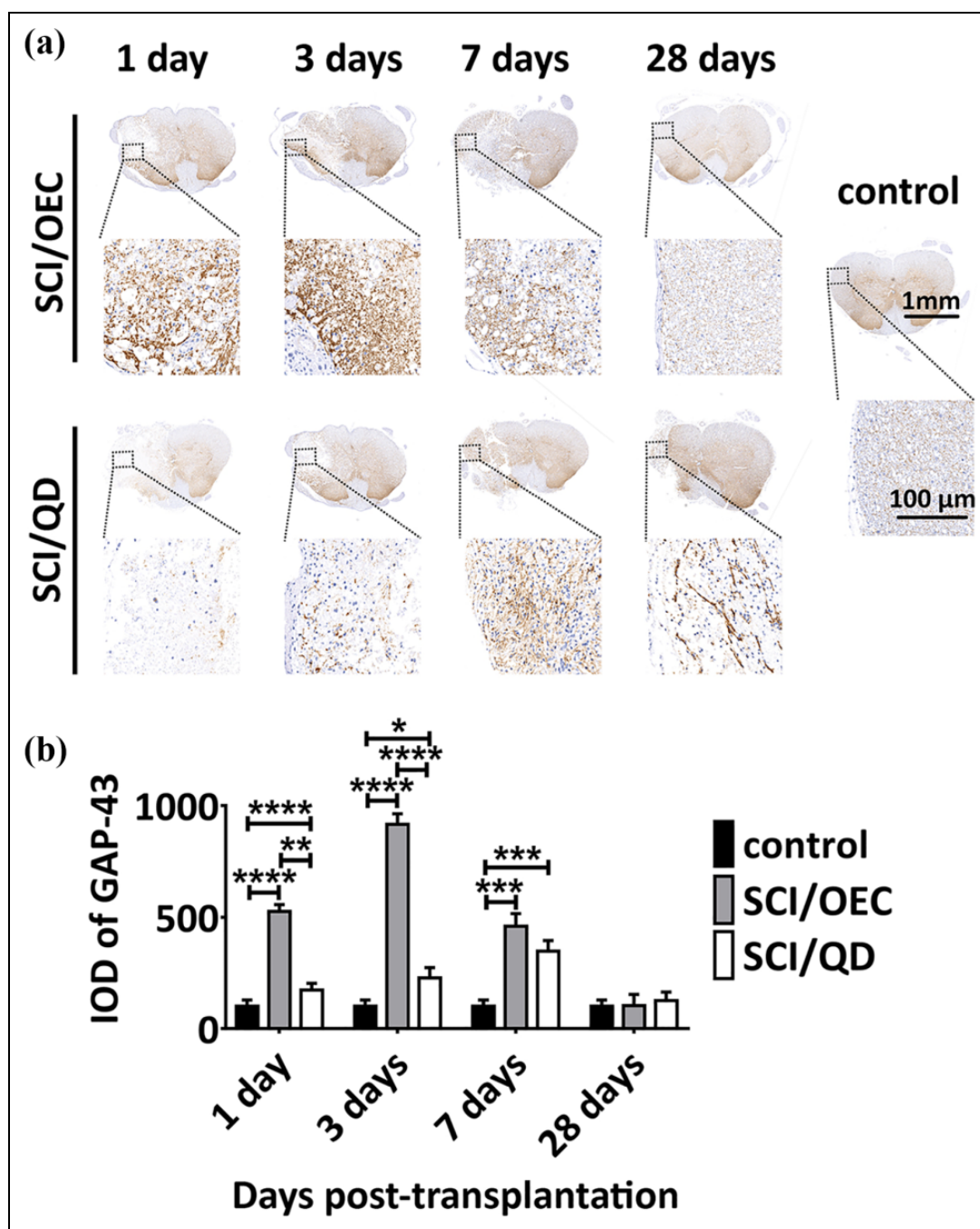
Figure 7. Exploration of the effect of OECs on axonal sprouting in the spinal cord after SCI. (a) GAP-43 immunostaining in the SCI/OEC, SCI/QD, and control groups at one day, three days, seven days, and 28 days after transplantation. (b) Average staining intensity (integrated optical density, IOD) of GAP-43 positive cells. Data are presented as mean $\pm$ SD, n = 5 per group. $*p < 0.05$; $**p < 0.01$; $***p < 0.001$; $****p < 0.0001$; scale bar = 100 μm, applicable to all sections.

Immunohistochemistry Analysis of Injured Spinal Cords

To investigate axonal growth after OEC treatment, immunostaining for growth-associated protein 43 (GAP-43; neuronal marker) was performed (Figure 7). Compared with rats in the SCI/QD group, SCI rats treated with OECs showed a markedly higher GAP-43 level, which was the highest at three days after OEC transplantation ($p < 0.005$; n = 5). These results indicated that OECs potentiated regenerative responses and facilitated axonal regeneration in the injured spinal cord.

To examine the effects of OECs on modulation of inflammatory responses, sections of spinal cord tissue were stained with Iba-1 antibody (microglia marker). In the control group, resting-state microglia with long cell processes were heterogeneously distributed in the gray matter and the white matter. In the SCI/QD group, the increased Iba-1 level was particularly evident within the injury epicenter and areas adjacent to the lesion site. The peak level of Iba-1 presented at seven days after transplantation. The activated microglia displayed enlarged cell bodies with short or thick processes. However, as shown in Figure 8, OEC treatment significantly decreased the activation of microglia compared with that in the SCI/QD group ($p < 0.001$; n = 5), with markedly lower Iba-1 levels detected at seven days after transplantation. At 28 days after injury, there was no significant difference between the Iba-1 level in the SCI/OEC group and in the control group ($p > 0.05$; n = 5). The data suggest that OECs could reduce the initial activation of Iba-1 positive immune cells and thereby contribute to tissue repair.

Demyelination is one of the major histopathologic hallmarks of SCI. In the present study, we evaluated the effects of OECs on the remyelination of the injured axons in the epicenter of the SCI by analysis of MBP (oligodendrocyte/myelin marker) (Figure 9). MBP staining showed a uniform pattern in the control group, whereas in the SCI/QD group, the mean IOD of MBP markedly decreased after SCI and reached the lowest level at seven days after transplantation ($p < 0.001$, n = 5). Then, the mean IOD of MBP gradually increased but was still significantly lower than that in the SCI/OEC group at 28 days after treatment ($p < 0.001$; n = 5). In the SCI/OEC group, the MBP levels were found to be significantly elevated at seven days after OEC treatment ($p < 0.001$, n = 5) and were slightly lower than the control group, but still statistically significant, at 28 days after transplantation ($p = 0.0215$, n = 5).

To determine the survival and migration of intravenously transplanted OECs, tissue sections stained with anti-p75 NGFR antibody were processed. As shown in Figure 10, in both the SCI/QD group and the control group, no p75 NGFR-positive cells were detected around the spinal cord injury site. In contrast, OECs were primarily found in regions close to the injury site in the SCI/OEC group. The IOD of p75 NGFR peaked at seven days after cell transplantation compared with other studied time points ($p < 0.0001$; n = 5).

Behavioral Outcome after OEC Treatment of Hemisection SCI Rats

BBB score was used to measure the motor function recovery of the SCI rats throughout the 28-day study period. The data showed a degree of spontaneous recovery of paw usage over time in all rats, regardless of OEC transplantation. However, the rats that received OEC transplantation showed the greatest improvement in locomotor function (Figure 11(a)). A significant difference began to appear at seven days after

cell treatment (7.33 ± 1.61 vs. 2.67 ± 0.58; $p = 0.011$; n = 5). As shown in Figure 11(b), extensive movement of all three joints of the hind limb, with sweeping or plantar placement of the paw with no weight support, was observed in the SCI/OEC group, whereas rats in the SCI/QD group were still dragging their hind legs with improved movement of the hip joint. These results suggest that the OEC transplantation could enhance the functional improvement of locomotor activity after SCI.

Discussion

Few studies have investigated the therapeutic role of olfactory bulb OECs and their biodistribution after systemic administration for treating SCI. Our results indicated the following. 1) OECs seem to be able to fulfill their neuroprotective roles at the injury site after an intravenous transplantation, leading to both functional and anatomical improvement. 2) After transplantation, labeled OECs were found at the injury site. 3) The accumulation of OECs was correlated with increasing BSCB permeability. The current study emphasizes the potential of the intravenous route for olfactory bulb OEC transplantation for the treatment of SCI.

1. The Therapeutic Roles of OECs in Tissue Regeneration of SCI

Our behavior tests presented a significant improvement of motor function in the SCI/OEC group compared with that in the SCI/QD group. Significant recovery of motor function began at seven days post-transplantation. Pathology studies were used to evaluate the therapeutic effects of intravenously injected OECs. The recovery of motor function was accompanied by a significant preservation of spinal cord parenchyma at the lesion site and increasing numbers of motor neurons in the anterior horn, which was shown in HE staining. The beneficial outcome was also confirmed with axonal outgrowth staining. Previous studies have documented that the high and transient elevation of GAP-43 in the damaged axons correlates with increased regenerative potential[38,39]. In our study, a dramatic increase in GAP-43 expression was observed in the OEC-treated rats compared with other groups as early as one day post-injection and peaked at three days post-injection. This may relate to the enhanced regenerative response for the axon in the damaged spinal cord after OEC treatment.

In the present study, the injured rats that received an intravenous injection of OECs exhibited a significant decrease in the infiltration of activated microglia, which were stained with Iba-1 antibody. This result suggested that the injected OECs could modulate the inflammatory response. The possible mechanism for the decreased neuroinflammation is partially due to the proinflammatory cytokines produced by the OECs. OECs are known to secrete anti-inflammatory factors, including CXCL12, interleukin 6 (IL-6), and CX3CL1, which can act on other immune cells,
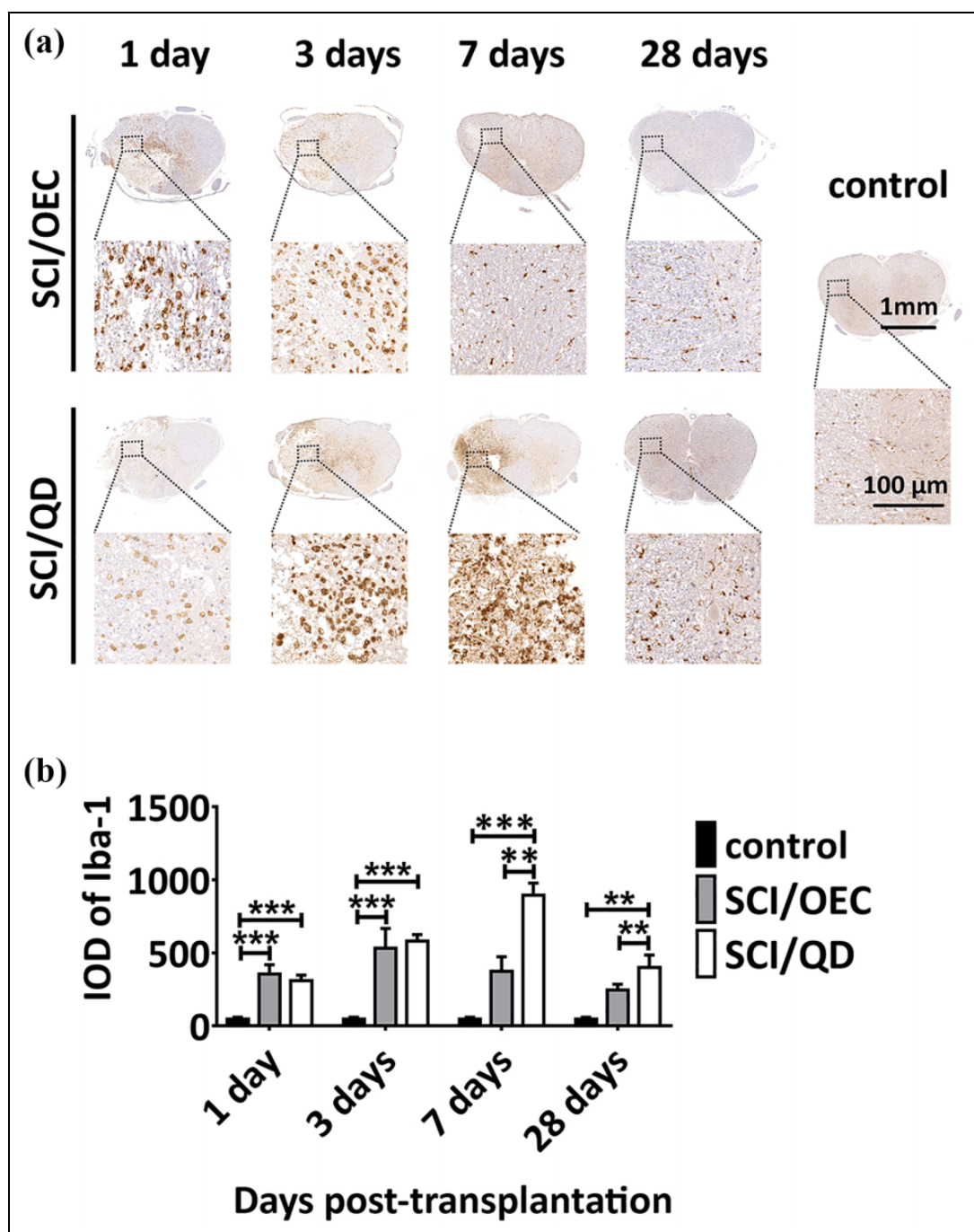
Figure 8. Protective role of OECs against neuroinflammation in the spinal cord after SCI. (a) Iba-1 immunostaining in the SCI/OEC, SCI/QD, and control groups at one day, three days, seven days, and 28 days after transplantation. (b) Average staining intensity (integrated optical density, IOD) of Iba-1 positive cells. Data are presented as mean $\pm$ SD, n = 5 per group. *p < 0.05; **p < 0.01; ***p < 0.001; scale bar = 100 μm, applicable to all sections.

such as neutrophils, macrophages, and lymphocytes, and phagocytose cellular debris after SCI[40].

Demyelination of spared axons also contributes to behavioral deficits by motor dysfunction and further secondary damage[41–44]. Among the myelin-producing cells, OEC transplantation has emerged as a promising repair strategy

due to their ability to modify the host environment to promote remyelination[45]. In this study, the remyelination of the injured axons was stained by MBP. The results showed that the remyelination was significantly higher in the SCI/OEC group than in the SCI/QD group, which confirmed that OECs were capable of remyelinating the demyelinated
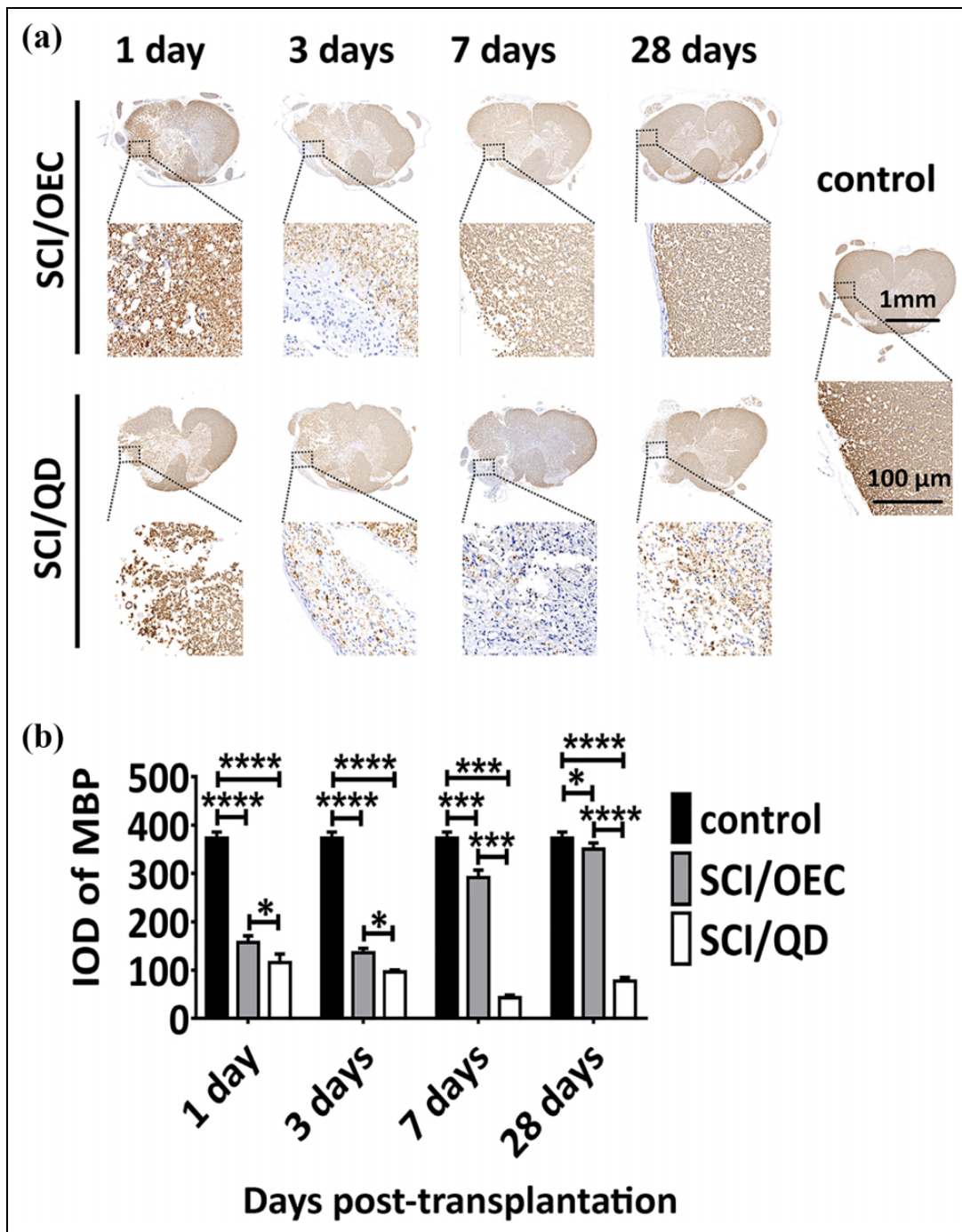
Figure 9. OECs promote remyelination in the spinal cord after SCI. (a) MBP immunostaining in the SCI/OEC, SCI/QD, and control groups at one day, three days, seven days, and 28 days after transplantation. (b) Average staining intensity (integrated optical density, IOD) of MBP positive cells. Data are presented as mean $\pm$ SD, n = 5 per group. *p < 0.05; **p < 0.01; ***p < 0.001; ****p < 0.0001; scale bar = 100 μm, applicable to all sections.

spared axons. Combined with the significant improvement of motor function in the SCI/OEC group, we speculated that the myelin regeneration induced by OECs could be an important contributor to the improvement in motor function. Their roles in improving the conduction velocity and frequency-response properties after SCI should be confirmed by the application of electroneurophysiology in a future study.

2. The Accumulation of Intravenously Transplanted OECs in the Injured Spinal Cord of Hemisection SCI Rats

The major challenge associated with cell-based therapy regarding SCI is to find the most cost-effective approaches to noninvasively deliver cells to the therapeutic targets. The
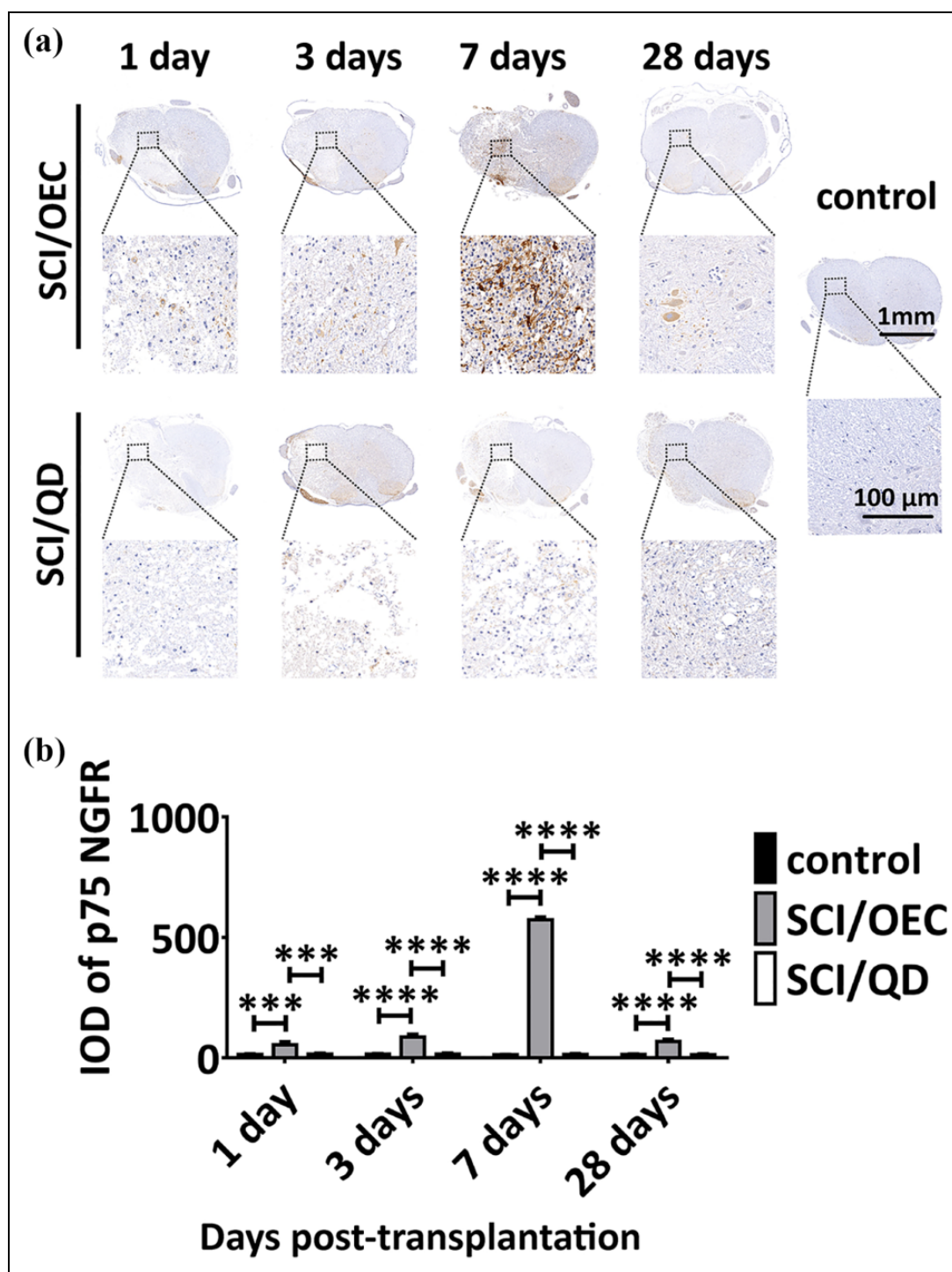
Figure 10. Immunostaining analysis showing the presence of transplanted OECs in the injured spinal cord. (a) Representative images of immunostaining for P75 NGFR at one day, three days, seven days, and 28 days after cell injection in the SCI/OEC, SCI/QD, and control groups. (b) Average staining intensity (integrated optical density, IOD) of P75 NGFR-positive regions in spinal cord sections. Data are presented as mean $\pm$ SD, n = 5 per group. *p < 0.05; **p < 0.01; ***p < 0.001; ****p < 0.0001; scale bar = 100 μm, applicable to all sections.

current strategies for transplantation of olfactory bulb OECs include intraspinal injection[46] and intrathecal administration[47]. Although these methods are acceptable for scientific studies in animals, they are difficult to implement in clinical practice for treating human SCI. The major limitation of these existing techniques is that they require complicated surgical procedures such as lumbar puncture or laminectomy to allow direct access to the spinal cord parenchyma, which
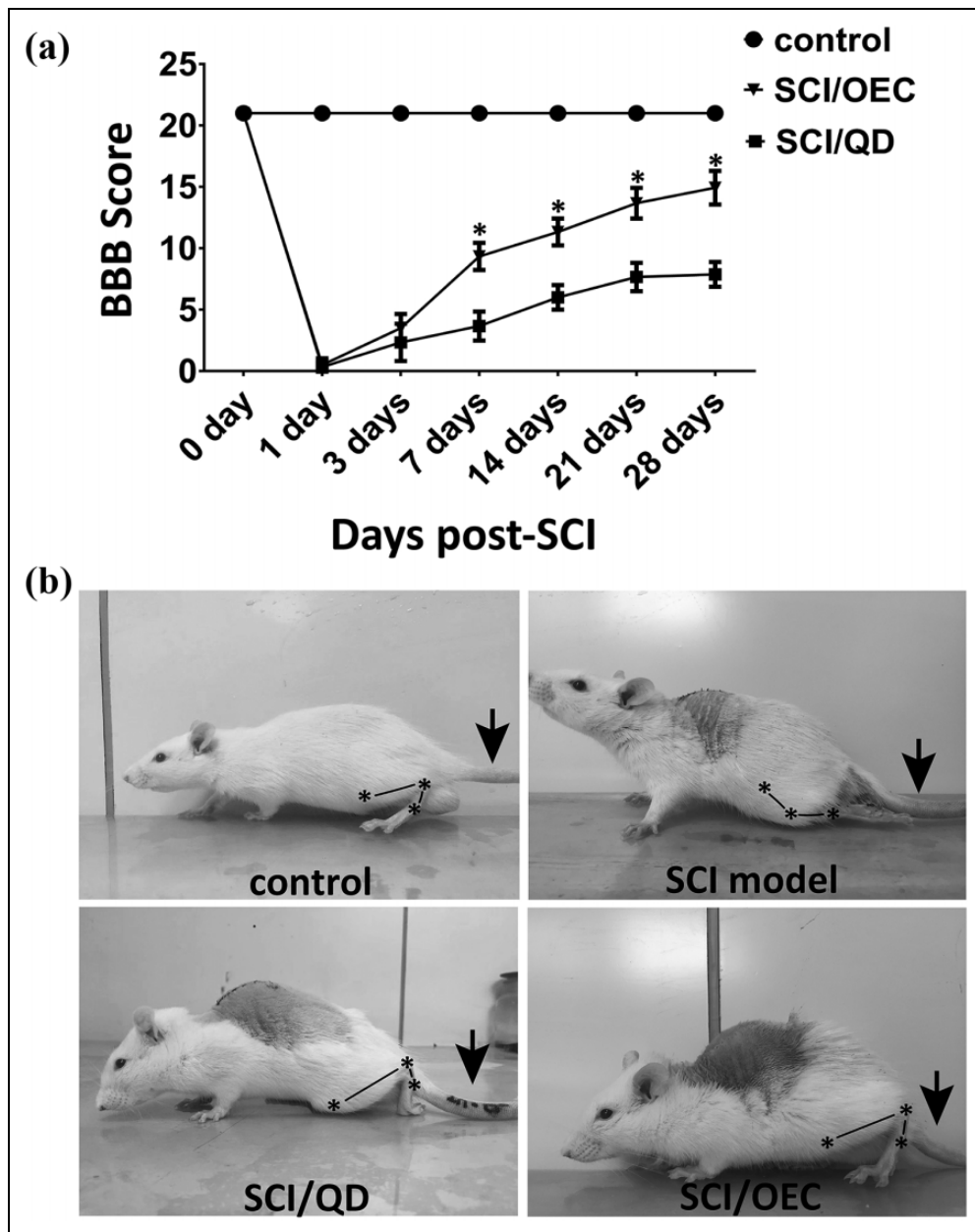
Figure 11. Motor function locomotion assessments of SCI rats. (a) BBB scoring. Values represent the mean $\pm$ SD (n $=$ 5). *p < 0.05 using one-way ANOVA followed by Tukey's tests. (b) Representative images from video recordings of one animal of every group for BBB scoring are shown as follows: control group; the SCI rat model; rat in the SCI/OEC group at seven days post-SCI; and rat in the SCI/QD group at seven days post-SCI. The black arrows indicate the tail position, and the stars represent the joints (the hip, knee, and ankle joints).

might cause further deterioration by damaging the remaining tissues or leading to several procedure-related complications. Previous evidence has reported that systemic transplantation, such as intravenous delivery of therapeutic cells, is relatively safe and easy to apply and can achieve equally beneficial results[48]. Therefore, we proposed that the transplanted olfactory bulb OECs could also promote the recovery of neurological function following intravenous transplantation. However, safe and successful bench-to-bedside translation calls for a more

comprehensive understanding of the in vivo cellular behaviors[49].

In this study, the spinal cord ex vivo imaging data showed that the QD-labeled OECs migrated into the injury site and started to accumulate only 10 min after intravenous injection. Seven days post-transplantation (eight days post-SCI), OECs accumulated in the injured spinal cord to their greatest extent, and thereafter decreased sharply. To confirm these optical imaging results, p75 NGFR immunostaining was carried out to locate the grafted OECs in the spinal tissue

sections. We found that the p75 NGFR-positive cells were detected near the injury site and in the dorsal root entry zone. We considered that the p75 NGFR-positive area located in the dorsal root entry zone was probably not from the grafted OECs, because p75 NGFR is always expressed in the neurons and glia of dorsal root ganglia[50,51]. In these areas, its expression is stable among different injury intervals and different groups. However, the p75 NGFR expression near the injury site in the SCI/OEC group was much higher than that in the SCI/QD group. Therefore, we speculate that the p75 NGFR near the injury site was expressed by OECs rather than representing a false-positive signal. The p75 NGFR expression increased after cell injection up to seven days post-injection. This finding indicated the increase of accumulated OECs in the injury site. However, the decrease of p75 NGFR expression at 14 days and 28 days post-injection was not only caused by the loss of OECs. Previous studies have indicated that p75 NGFR expression can be regulated by interactions with extrinsic factors such as axonal contact. After transplantation into CNS tissue, p75 NGFR-positive OECs ensheathed neurites and then lost p75 NGFR expression on their membranes where they were in direct contact with the neurites[52,53].

The biodistribution results showed that OECs mainly accumulate in the liver. However, some results showed that substantial amounts of other types of intravenously injected cells were entrapped within pulmonary capillaries[54,55]. These discrepant results might arise from the differences in cell size, cell type, and the immune state of the host[56,57]. Moreover, the fluorescence imaging method has its own limitations; for example, it is difficult to quantify the photon number of isolated organs because of the differences in the optical properties of different organs. The thickness and positioning may also affect the results[58,59].

Monitoring OEC distribution by using QDs is not without flaws. For example, it is possible that the fluorescence signal we detected was from the QDs released by dead cells. Nevertheless, combined with improvement in motor function and pathology studies, it is more likely that the intravenously injected OECs could accumulate in the spinal cord through a disrupted BSCB. However, further studies are required to visualize cell viability and migration using specific noninvasive imaging methods. In particular, reporter gene imaging, such as herpes simplex virus type 1 thymidine kinase (HSV1-tk), can be used to evaluate biological processes of the transplanted cells at the cellular and molecular levels in vivo[60].

3. Intravenously Injected OECs Penetrated the Injury Epicenter through Disrupted BSCB

Regenerative medicine using cell-based therapy has recently emerged as a viable therapeutic approach for treating CNS injuries and degenerative diseases[61]. Unfortunately, the presence of the BSCB limits or blocks the entrance of potential treatments (i.e., drugs, trophic factors, and curative cells) to the spinal cord parenchyma and the exchange between the bloodstream and the spinal cord environment[62,63]. After SCI, a compromised BSCB could provide a unique opportunity for therapeutic interventions[64]. The BSCB permeability in this study was assessed by ex vivo imaging and spectrophotometric quantification of the content of EvB leakage in the injury site. The BSCB was disrupted as early as 10 min post-SCI, with the maximum permeability occurring around seven days after the establishment of the hemisection rat model. There was a positive correlation between the fluorescence signal of OECs at the injury site and the EvB leakage in the damaged spinal cord. Therefore, we proposed that the number of OECs migrating into the epicenter of trauma is highly related to the permeability of the BSCB. In future work, the time window of OEC transplantation should be optimized according to the BSCB permeability.

Previous groups have characterized and investigated the permeability of BSCB and the possible underlying mechanisms[65,66]. However, the results were inconsistent regarding the time window of BSCB opening. This variability might be due to the varying severity of injury, edema formation, or the type of SCI animal model used, such as contusion SCI models[67,68], while a hemisection at T12 rat model was employed here.

Conclusion

Intravenous transplantation is a minimally invasive method for OEC transplantation for the repair of SCI. In this study, we investigated the distribution and function of intravenously injected olfactory bulb OECs in the intact and injured spinal cord. Our results showed that the grafted OECs colonized damaged spinal cord tissue, which was important for remyelination, modulating neuroinflammation, and tissue preservation. The BSCB opening pattern was closely correlated with the migration of QD-labeled OECs in the injured spinal cord. We believe that OECs migrated into the parenchyma of the spinal cord by penetrating the disrupted BSCB. Therefore, the penetrability of the BSCB could provide the clinically relevant time window for cell transplantation therapy in the treatment of SCI.

Ethical Approval

This study was approved by our institutional review board.

Statement of Human and Animal Rights

This article does not contain any studies with human subjects. All pr10.1177/0963689719883842ocedures with animal subjects in this study were conducted in accordance with the Ningxia Medical University Animal Ethics Committee, Ningxia Medical University, Yinchuan, China.

Statement of Informed Consent

There are no human subjects in this article and informed consent is not applicable.

Declaration of Conflicting Interests

Funding

ORCID iD

Xiaoqing Zhuang ⬦ https://orcid.org/0000-0001-8652-8540

Supplemental Material

Supplemental material for this article is available online.

References

1. Thuret S, Moon LD, Gage FH. Therapeutic interventions after spinal cord injury. Nat Rev Neurosci. 2006;7(8):628–643.

2. Awai L, Bolliger M, Ferguson AR, Courtine G, Curt A. Influence of spinal cord integrity on gait control in human spinal cord injury. Neurorehabil Neural Repair. 2016;30(6):562–572.

3. Lee BB, Cripps RA, Fitzharris M, Wing PC. The global map for traumatic spinal cord injury epidemiology: update 2011, global incidence rate. Spinal Cord. 2014;52(2):110–116.

4. Fouad K, Tetzlaff W. Rehabilitative training and plasticity following spinal cord injury. Exp Neurol. 2012;235(1):91–99.

5. Hand BN, Krause JS, Simpson KN. Polypharmacy and adverse drug events among propensity score matched privately insured persons with and without spinal cord injury. Spinal Cord. 2018; 56(6):591–597.

6. Centenaro LA, Jaeger Mda C, Ilha J, de Souza MA, Kalil-Gaspar PI, Cunha NB, Marcuzzo S, Achaval M. Olfactory and respiratory lamina propria transplantation after spinal cord transection in rats: effects on functional recovery and axonal regeneration. Brain Res. 2011;1426:54–72.

7. Witheford M, Westendorf K, Roskams AJ. Olfactory ensheathing cells promote corticospinal axonal outgrowth by a L1 CAM-dependent mechanism. Glia. 2013;61(11):1873–1889.

8. Ruiz-Mendoza S, Macedo-Ramos H, Santos FA, Quadros-de-Souza LC, Paiva MM, Pinto TC, Teixeira LM, Baetas-da-Cruz W. Streptococcus pneumoniae infection regulates expression of neurotrophic factors in the olfactory bulb and cultured olfactory ensheathing cells. Neuroscience. 2016;317:149–161.

9. Bonfanti R, Musumeci T, Russo C, Pellitteri R. The protective effect of curcumin in olfactory ensheathing cells exposed to hypoxia. Eur J Pharmacol. 2017;796:62–68.

10. López-Vales R, García-Alías G, Forés J, Vela JM, Navarro X, Verdú E. Transplanted olfactory ensheathing cells modulate the inflammatory response in the injured spinal cord. Neuron Glia Biol. 2004;1(3):201–209.

11. Sasaki M, Lankford KL, Radtke C, Honmou O, Kocsis JD. Remyelination after olfactory ensheathing cell transplantation into diverse demyelinating environments. Exp Neurol. 2011; 229(1):88–98.

12. Féron F, Perry C, Cochrane J, Licina P, Nowitzke A, Urquhart S, Geraghty T, Mackay-Sim A. Autologous olfactory ensheathing cell transplantation in human spinal cord injury. Brain. 2005;128 (Pt 12):2951–2960.

13. Ramon-Cueto A, Munoz-Quiles C. Clinical application of adult olfactory bulb ensheathing glia for nervous system repair. Exp Neurol. 2011;229(1):181–194.

14. Yamamoto M, Raisman G, Li D, Li Y. Transplanted olfactory mucosal cells restore paw reaching function without regeneration of severed corticospinal tract fibres across the lesion. Brain Res. 2009;1303:26–31.

15. Ibrahim A, Li D, Collins A, Tabakow P, Raisman G, Li Y. Comparison of olfactory bulbar and mucosal cultures in a rat rhizotomy model. Cell Transplant. 2014;23(11):1465–1470.

16. Gómez RM, Ghotme K, Botero L, Bernal JE, Pérez R, Barreto GE, Bustos RH. Ultrastructural analysis of olfactory ensheathing cells derived from olfactory bulb and nerve of neonatal and juvenile rats. Neurosci Res. 2016;103:10–17.

17. Pellitteri R, Russo A, Stanzani S, Zaccheo D. Olfactory ensheathing cells protect cortical neuron cultures exposed to hypoxia. CNS Neurol Disord Drug Targets. 2015;14(1):68–76.

18. Radtke C, Akiyama Y, Brokaw J, Lankford KL, Wewetzer K, Fodor WL, Kocsis JD. Remyelination of the nonhuman primate spinal cord by transplantation of H-transferase transgenic adult pig olfactory ensheathing cells. FASEB J. 2004;18(2): 335–337.

19. Tabakow P, Raisman G, Fortuna W, Czyz M, Huber J, Li D, Szewczyk P, Okurowski S, Miedzybrodzki R, Czapiga B, Salomon B, et al. Functional regeneration of supraspinal connections in a patient with transected spinal cord following transplantation of bulbar olfactory ensheathing cells with peripheral nerve bridging. Cell Transplant. 2014;23(12):1631–1655.

20. Czyz M, Tabakow P, Hernandez-Sanchez I, Jarmundowicz W, Raisman G. Obtaining the olfactory bulb as a source of olfactory ensheathing cells with the use of minimally invasive neuroendoscopy-assisted supraorbital keyhole approach–cadaveric feasibility study. Br J Neurosurg. 2015;29(3):362–370.

21. Miedzybrodzki R, Tabakow P, Fortuna W, Czapiga B, Jarmundowicz W. The olfactory bulb and olfactory mucosa obtained from human cadaver donors as a source of olfactory ensheathing cells. Glia. 2006;54(6):557–565.

22. Liadi M, Collins A, Li Y, Li D. The impact of tissue storage conditions on rat olfactory ensheathing cell yield and the future clinical implications. Cell Transplant. 2018;27(9):1320–1327.

23. Woodhall E, West AK, Chuah MI. Cultured olfactory ensheathing cells express nerve growth factor, brain-derived neurotrophic factor, glia cell line-derived neurotrophic factor and their receptors. Brain Res Mol Brain Res. 2001;88(1–2): 203–213.

24. Srivastava AK, Bulte JW. Seeing stem cells at work in vivo. Stem Cell Rev. 2014;10(1):127–144.

25. Gleave JA, Valliant JF, Doering LC. [99]mTc-based imaging of transplanted neural stem cells and progenitor cells. J Nucl Med Technol. 2011;39(2):114–120.

26. Dunning MD, Lakatos A, Loizou L, Kettunen M, ffrench-Constant C, Brindle KM, Franklin RJ. Superparamagnetic iron oxide-labeled Schwann cells and olfactory ensheathing cells can be traced in vivo by magnetic resonance imaging and retain functional properties after transplantation into the CNS. J Neurosci. 2004;24(44):9799–9810.

27. Michalet X, Pinaud FF, Bentolila LA, Tsay JM, Doose S, Li JJ, Sundaresan G, Wu AM, Gambhir SS, Weiss S. Quantum dots for live cells, in vivo imaging, and diagnostics. Science. 2005; 307(5709):538–544.

28. Sugaya H, Mishima H, Gao R, Kaul SC, Wadhwa R, Aoto K, Li M, Yoshioka T, Ogawa T, Ochiai N, Yamazaki M. Fate of bone marrow mesenchymal stromal cells following autologous transplantation in a rabbit model of osteonecrosis. Cytotherapy. 2016;18(2):198–204.

29. Rosenthal SJ, Chang JC, Kovtun O, McBride JR, Tomlinson ID. Biocompatible quantum dots for biological applications. Chem Biol. 2011;18(1):10–24.

30. Nash HH, Borke RC, Anders JJ. New method of purification for establishing primary cultures of ensheathing cells from the adult olfactory bulb. Glia. 2001;34(2):81–87.

31. Wang J, Zhang L, Xia H, Liang X, Wang Y. Effect of autophagy induced by hypoxia on cell proliferation in olfactory ensheathing cells from olfactory mucosa of rats. J Jilin Univ Med Ed. 2016;42(03):430–434.

32. Chibli H, Carlini L, Park S, Dimitrijevic NM, Nadeau JL. Cytotoxicity of InP/ZnS quantum dots related to reactive oxygen species generation. Nanoscale. 2011;3(6):2552–2559.

33. Saxena T, Deng B, Stelzner D, Hasenwinkel J, Chaiken J. Raman spectroscopic investigation of spinal cord injury in a rat model. J Biomed Opt. 2011;16(2):027003.

34. Santiago JM, Rosas O, Torrado AI, González MM, Kalyan-Masih PO, Miranda JD. Molecular, anatomical, physiological, and behavioral studies of rats treated with buprenorphine after spinal cord injury. J Neurotrauma. 2009;26(10):1783–1793.

35. Basso DM, Beattie MS, Bresnahan JC. A sensitive and reliable locomotor rating scale for open field-testing in rats. J Neurotrauma. 1995;12(1):1–21.

36. Chen H, Li J, Liang S, Lin B, Peng Q, Zhao P, Cui J, Rao Y. Effect of hypoxia-inducible factor-1/vascular endothelial growth factor signaling pathway on spinal cord injury in rats. Exp Ther Med. 2017;13(3):861–866.

37. Sotoudeh A, Jahanshahi A, Zareiy S, Darvishi M, Roodbari N, Bazzazan A. The influence of low-level laser irradiation on spinal cord injuries following ischemia-reperfusion in rats. Acta Cir Bras. 2015;30(9):611–616.

38. Curtis R, Averill S, Priestley JV, Wilkin GP. The distribution of GAP-43 in normal rat spinal cord. J Neurocytol. 1993;22(1): 39–50.

39. Teng YD, Lavik EB, Qu X, Park KI, Ourednik J, Zurakowski D, Langer R, Snyder EY. Functional recovery following traumatic spinal cord injury mediated by a unique polymer scaffold seeded with neural stem cells. Proc Natl Acad Sci U S A. 2002; 99(5):3024–3029.

40. Chuah MI, Hale DM, West AK. Interaction of olfactory ensheathing cells with other cell types in vitro and after transplantation: glial scars and inflammation. Exp Neurol. 2011; 229(1):46–53.

41. Papastefanaki F, Matsas R. From demyelination to remyelination: the road toward therapies for spinal cord injury. Glia. 2015;63(7):1101–1125.

42. Plemel JR, Keough MB, Duncan GJ, Sparling JS, Yong VW, Stys PK, Tetzlaff W. Remyelination after spinal cord injury: is it a target for repair? Prog Neurobiol. 2014;117:54–72.

43. Lang EJ, Rosenbluth J. Role of myelination in the development of a uniform olivocerebellar conduction time. J Neurophysiol. 2003;89(4):2259–2270.

44. Nickel M, Gu C. Regulation of central nervous system myelination in higher brain functions. Neural Plast. 2018;2018: 6436453.

45. Santos-Benito FF, Ramón-Cueto A. Olfactory ensheathing glia transplantation: a therapy to promote repair in the mammalian central nervous system. Anat Rec B New Anat. 2003;271(1): 77–85.

46. Khankan RR, Griffis KG, Haggerty-Skeans JR, Zhong H, Roy RR, Edgerton VR, Phelps PE. Olfactory ensheathing cell transplantation after a complete spinal cord transection mediates neuroprotective and immunomodulatory mechanisms to facilitate regeneration. J Neurosci. 2016;36(23):6269–6286.

47. Liu T, Ji ZQ, Ahsan SM, Zhang Y, Zhang P, Fan ZH, Shen YX. Intrathecal transplantation of olfactory ensheathing cells by lumbar puncture for thoracic spinal cord injury in mice. J Neurorestoratology. 2017;5:103–109.

48. White SV, Czisch CE, Han MH, Plant CD, Harvey AR, Plant GW. Intravenous transplantation of mesenchymal progenitors distribute solely to the lungs and improve outcomes in cervical spinal cord injury. Stem Cells. 2016;34(7):1812–1825.

49. Holvoet B, De Waele L, Quattrocelli M, Gheysens O, Sampaolesi M, Verfaillie CM, Deroose CM. Increased understanding of stem cell behavior in neurodegenerative and neuromuscular disorders by use of noninvasive cell imaging. Stem Cells Int. 2016;2016:6235687.

50. Li Y, Carlstedt T, Berthold CH, Raisman G. Interaction of transplanted olfactory ensheathing cells and host astrocytic processes provides a bridge for axons to regenerate across the dorsal root entry zone. Exp Neurol. 2004;188(2):300–308.

51. Pascual JI, Gudiño-Cabrera G, Insausti R, Nieto-Sampedro M. Spinal implants of olfactory ensheathing cells promote axon regeneration and bladder activity after bilateral lumbosacral dorsal rhizotomy in the adult rat. J Urol. 2002;167(3): 1522–1526.

52. Ramón-Cueto A, Pérez J, Nieto-Sampedro M. In vitro enfolding of olfactory neurites by p75 NGF receptor positive ensheathing cells from adult rat olfactory bulb. Eur J Neurosci. 1993;5(9):1172–1180.

53. Wewetzer K, Kern N, Ebel C, Radtke C, Brandes G. Phagocytosis of O4+ axonal fragments in vitro by p75-neonatal rat olfactory ensheathing cells. Glia. 2005;49(4):577–587.

54. Fischer UM, Harting MT, Jimenez F, Monzon-Posadas WO, Xue H, Savitz SI, Laine GA, Cox CS Jr. Pulmonary passage is a major obstacle for intravenous stem cell delivery: the pulmonary first-pass effect. Stem Cells Dev. 2009;18(5): 683–692.

55. Schrepfer S, Deuse T, Reichenspurner H, Fischbein MP, Robbins RC, Pelletier MP. Stem cell transplantation: the lung barrier. Transplant Proc. 2007;39(2):573–576.

56. Scarfe L, Taylor A, Sharkey J, Harwood R, Barrow M, Comenge J, Beeken L, Astley C, Santeramo I, Hutchinson C, Ressel L, et al. Non-invasive imaging reveals conditions that impact distribution and persistence of cells after in vivo administration. Stem Cell Res Ther. 2018;9(1):332.

57. Leibacher J, Henschler R. Biodistribution, migration and homing of systemically applied mesenchymal stem/stromal cells. Stem Cell Res Ther. 2016;7:7.

58. Virostko J, Chen Z, Fowler M, Poffenberger G, Powers AC, Jansen ED. Factors influencing quantification of in vivo bioluminescence imaging: application to assessment of pancreatic islet transplants. Mol Imaging. 2004;3(4): 333–342.

59. Schmuck EG, Koch JM, Centanni JM, Hacker TA, Braun RK, Eldridge M, Hei DJ, Hematti P, Raval AN. Biodistribution and clearance of human mesenchymal stem cells by quantitative three-dimensional cryo-imaging after intravenous infusion in a rat lung injury model. Stem Cells Transl Med. 2016;5(12): 1668–1675.

60. Pei Z, Zeng J, Song Y, Gao Y, Wu R, Chen Y, Li F, Li W, Zhou H, Yang Y. In vivo imaging to monitor differentiation and therapeutic effects of transplanted mesenchymal stem cells in myocardial infarction. Sci Rep. 2017;7(1):6296.

61. Metcalfe SM, Bickerton S, Fahmy T. Neurodegenerative disease: a perspective on cell-based therapy in the new era of cell-free nano-therapy. Curr Pharm Des. 2017;23(5):776–783.

62. Gonzales-Portillo GS, Sanberg PR, Franzblau M, Gonzales-Portillo C, Diamandis T, Staples M, Sanberg CD, Borlongan CV. Mannitol-enhanced delivery of stem cells and their growth factors across the blood-brain barrier. Cell Transplant. 2014; 23(4-5):531–539.

63. Banks WA. From blood-brain barrier to blood-brain interface: new opportunities for CNS drug delivery. Nat Rev Drug Discov. 2016;15(4):275–292.

64. Figley SA, Khosravi R, Legasto JM, Tseng YF, Fehlings MG. Characterization of vascular disruption and blood-spinal cord barrier permeability following traumatic spinal cord injury. J Neurotrauma. 2014;31(6):541–552.

65. Tatar I, Chou PC, Desouki MM, El Sayed H, Bilgen M. Evaluating regional blood spinal cord barrier dysfunction following spinal cord injury using longitudinal dynamic contrast-enhanced MRI. BMC Med Imaging. 2009;9:10.

66. Lee JY, Kim HS, Choi HY, Oh TH, Ju BG, Yune TY. Valproic acid attenuates blood-spinal cord barrier disruption by inhibiting matrix metalloprotease-9 activity and improves functional recovery after spinal cord injury. J Neurochem. 2012;121(5):818–829.

67. Whetstone WD, Hsu JY, Eisenberg M, Werb Z, Noble-Haeusslein LJ. Blood-spinal cord barrier after spinal cord injury: relation to revascularization and wound healing. J Neurosci Res. 2003; 74(2):227–239.

68. Popovich PG, Horner PJ, Mullin BB, Stokes BT. A quantitative spatial analysis of the blood-spinal cord barrier. I. Permeability changes after experimental spinal contusion injury. Exp Neurol. 1996;142(2):258–275.